Electrochimica Acta 124 (2014) 211–217

Contents lists available at ScienceDirect

Electrochimica Acta

journal homepage: www.elsevier.com/locate/electacta

Analysis of AISI 1020 steel corrosion in seawater by coupling electrochemical noise and optical microscopy

Emerson C. Rios*, Alexsandro M. Zimer, Ernesto C. Pereira, Lucia H. Mascaro*

Laboratório Interdisciplinar de Eletroquímica e Cerâmica (LIEC), Federal University of São Carlos (UFSCar), Chemistry Dept., C.P.: 676, CEP: 13.565-905, São Carlos, SP, Brazil[1]

ARTICLE INFO

Article history:
Received 14 March 2013
Received in revised form
28 September 2013
Accepted 9 October 2013
Available online 4 November 2013

Keywords:
Corrosion
Seawater
Electrochemical noise
Wavelets

ABSTRACT

Electrochemical noise coupled to in situ optical micrographs was used to study corrosion processes in AISI 1020 steel immersed in seawater. The noise data was analysed using wavelet transform. The results were represented in energy diagrams and showed that considerable changes occurred in the corrosion mechanism during the initial step of the experiment (until 7200 s). During this initial step, it was observed that the corrosion was predominantly localized by means of pitting formation and intergranular corrosion. After approximately 50,000 s (14 h) of immersion, general corrosion processes become dominant. The conclusions obtained from the analysis of the current noise signal using the wavelet transform were confirmed by optical micrograph which suggests that the coupling of electrochemical noise and optical microscopy techniques can be valuable in studying corrosion processes in this system. Another advantage of this procedure is the elucidation and separation of corrosion processes, such as, for example, pitting and intergranular ones, that are not commonly identified by other techniques.

1. Introduction

Carbon steel generally presents surface defects, such as grain boundaries and inclusions, which are the preferred sites for the initiation of pitting corrosion [1]. Among the different corrosion kinds, localized corrosion is frequently observed in chloride media, and is the most difficult one to detect and monitor using conventional electrochemical techniques, such as open circuit potential and/or polarisation curves.

A different approach to investigate pitting formation is the electrochemical noise (ECN) method. ECN can be defined as random fluctuations of the current and/or potential observed in an electrochemical system [2]. From the literature, it is commonly accepted that electrochemical noise is usually a result of changes in the surface states of a metallic electrode, such as, for example, the breakdown and repair of a surface film [3–7]. Therefore, ECN provides valuable information about complex electrochemical reactions in a non-stationary condition. This fact enables the method to be applied in the study of environment-assisted cracks [8–10], pitting [7,11–13], grain boundaries [12,14] and general corrosion [10,15]. The experiments are generally performed under open circuit potential condition, E_{oc}, using two symmetric working electrodes, WE_1 and WE_2, and a reference electrode, RE. The current noise signal, I_n, is measured between the working electrodes and potential noise, V_n, is determined between the working and reference electrodes.

Different mathematical methods can be used for the deconvolution of the ECN signal, such as Fourier [5] and wavelet transforms [16]. This latter procedure has been proposed as an alternative tool that is able to overcome the limitations of the Fourier transform in which the coefficients are obtained by correlating the original signal with sine and cosine wave functions. Hence, the use of Fourier analysis is suitable for processing stationary signals once Fourier transform specifies the frequency content of the signal but does not provide information about the position in the time domain at the point when these frequencies are emitted. On the other hand, the wavelet transform is indicated for the study of both stationary and non-stationary ECN time data [16], and for analysing the different ECN components which contributes to the original signal. Each component is defined by a set of wavelet coefficients that contain information about the timescale characteristics of the associated corrosion event. Generally, the interpretation is undertaken using energy distribution plots (EDPs) [6,12,16–18]. In this case, specifically considering corrosion data, it is possible to differentiate, both qualitatively and quantitatively, between two or more corrosion processes that are simultaneously present in the system. The disadvantage of this approach is the lack of information about the surface spatial coordinates once there is no description of the points on the

* Corresponding authors. Tel.: +55 16 3351 9452.
E-mail addresses: emersoncostarios@yahoo.com.br (E.C. Rios)
lmascaro@ufscar.br (L.H. Mascaro).
[1] Tel.: +55 16 33519309; fax: +55 16 33615215.

0013-4686/$ – see front matter © 2013 Elsevier Ltd. All rights reserved.
http://dx.doi.org/10.1016/j.electacta.2013.10.059

surface where the corrosion occurs. This is a consequence of the fact that the current and potential are associated with the sum of all the events that take place on the electrode [19].

Pits are generally small and they can only be viewed using at least a magnifying glass or an optical microscope. The development of techniques to access the details of pitting corrosion is therefore an important challenge. There are few papers in the literature that describe localized corrosion information in terms of spatial position over a surface using real-time measurements, or which correlate information with data obtained using a second technique [17,20–25]. Li et al. [21] used an in situ atomic force microscope (AFM) and ECN techniques to investigate the corrosion initiation process on 1Cr18Ni9Ti stainless steel immersed in a 0.5 M HCl solution. The electrochemical current noise data were analysed using discrete wavelet transform, and the origin of the wavelet coefficients was discussed based on the correlation between the evolution of the energy distribution plot and on the topographic changes. The authors found that the initiation of metastable pitting at susceptible sites, in diluted HCl solution, is a result of the breakdown of the stainless steel passive film. Budiansky et al. [20] used spatial point pattern analysis method to characterise the spatial distribution of pitting on AISI 316 stainless steel. Experimental pitting on that steel was analysed using optical microscopy, indicating the existence of interactions between micrometre-scale pits over multiple pit distances. The spatial statistics additionally indicated an interaction among the pit rate growth when they are formed under potentiodynamic conditions. Finally, the authors proposed that the acid/halide pitting mechanism also leads to an interaction between pit sites. Yin et al. [22] used scanning electrochemical microscopy (SECM) to investigate the localized corrosion of 304 stainless steel in neutral chloride solution. The authors described a relationship between the local ion concentration and the electrochemical activity species involved in the corrosion reaction. The SECM measurements were also employed for in situ study of the composition and electrochemical activity distribution profile of the pitting corrosion products. This last fact demonstrated that the combination of the feedback current mode and generation-collection (G-C) mode of SECM was appropriate for elucidating the possible reaction mechanisms and paths involved in the localized corrosion.

With the objective of studying the initial stages of the corrosion of AISI 1020 steel in seawater, the present study employed electrochemical noise measurements coupled with in situ optical microscopy. This last technique enables the determination of the spatial coordinates where the corrosion occurs. We used wavelet transform and energy diagram plots to interpret current noise, enabling both a qualitative and quantitative analysis to be made of the changes occurring during the onset of this type corrosion.

2. Experimental

The working electrodes used were commercially available AISI 1020 steel (0.186% C, 0.022% Cr, 0.017% Cu, 0.509% Mn, 0.002% Mo, 0.013% Ni, 0.003% P, 0.030% S, 0.106% Si, balance Fe in wt.%) supplied in the form of rods. The samples were annealed at 900 °C for 60 min. After, the sample' microstructure was studied using optical microscopy. The metallographic sample preparation for observations consisted of grinding down to 1200-grit paper, followed by 0.25 μm diamond paste. After polishing, the samples were etched for 10 s in Nital 2.0% solution. Fig. 1 presents the sample after the annealing treatment. As can be shown, the metallic surface is composed by inclusions with size less than 1 micron distributed over the ferritic grains. Regarding the phase composition, the sample present approximately 17% pearlitic and 83% of ferritic phases, respectively.

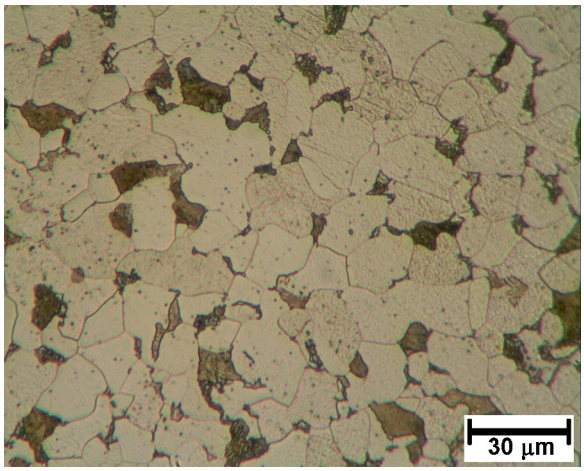

Fig. 1. Microstructure of the AISI 1020 steel annealed at 900 °C for 60 min and air quenched. Etching: Nital 2.0%.

Two identical samples, WE_1 and WE_2, with area = 0.5 mm^2, were embedded in polyester resin side by side, separated by 1 cm. The purpose to use a very small area working electrode is to enable the visualization of the total surface using optical microscopy. The assemblage was polished with 1200-grit sandpaper followed by a 0.25 μm diamond paste. The electrodes were cleaned in Extran® 5% and then with acetone in an ultrasound bath. A saturated Ag/AgCl/KCl reference electrode, RE, was used in the electrochemical experiments, i.e., potential and current noise data were collected simultaneously. The composition of artificial seawater is shown in Table 1 and was prepared in accordance with Lyman and Fleming [26].

An Autolab-PGSTAT20, with the ECN module controlled by NOVA 1.6 software, was used to perform the ECN measurements under E_{oc} conditions. The measurement was performed at constant room temperature (25 °C). Noise was registered at a sampling frequency of f_s = 6 Hz. The signal analysis was performed using appropriate software, and the Daubechies-wavelets "db4" orthogonal function was applied in eight levels of decomposition. The main property of the chosen function is that the energy of the analysed signal is equal to the sum of the energies of all components obtained by the wavelet transform; these look like fractal-type signals and a faster convergence of wavelet coefficients is therefore expected. We interpreted the results in the present study by estimating the energy contribution of each level of decomposition in relation to the original signal. This type of analysis is well described by Aballe et al. [16].

The electrodes were mounted in a flat-bottom electrochemical cell, which was positioned over the ocular of an inverted optical microscope (Opton model TNM-07T-PL), in order to perform in situ image acquisition, as depicted in Fig. 2. The images of the WE_1 surface were collected at 200× magnification using the program Scope

Table 1
Composition of synthetic seawater for 1 l.

Addition order	Reagent	Quantity
1	NaF	3.0 mg
2	$SrCl_2{\cdot}6H_2O$	20.0 mg
3	H_3BO_3	30.0 mg
4	Na_2SO_4	4000 mg
5	$CaCl_2$	1113 mg
6	$MgCl_2{\cdot}6H_2O$	10,780 mg
7	KBr	100 mg
8	KCl	700 mg
9	NaCl	23,500 mg
10	$NaHCO_3$	200 mg

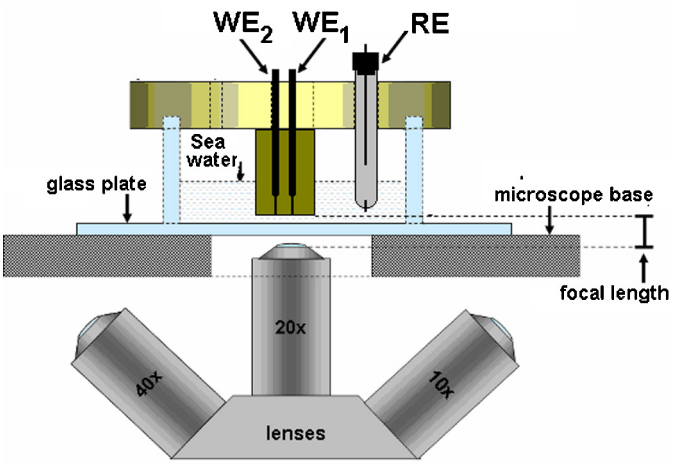

Fig. 2. Schematic diagram of the simultaneous optical and electrochemical measurements.

Photo® 1.0, and with an image acquisition rate of one frame every 2 s at a resolution of 1280 × 1024 pixels. This setup allowed optical measurements and electrochemical experiments to be performed simultaneously. Tests were performed in duplicate.

3. Results and discussion

Immediately after immersing the electrodes in the solution, both V_n and I_n were measured using the setup described above. An oscillation of 10^{-4} V and 10^{-8} A was observed for the potential and current, respectively. Papers in the literature [27,28] propose that the intensity of the noise is related to pit formation. In this case, abrupt changes in the potential and/or current are related to local destruction of the passive layer, followed by repassivation leading to a decrease in I_n to lower values again. In the case of potential noise, it has been proposed that these values are related to the capacitance of the metal/solution interface [28]. Then, to follow the corrosion process, was decided to study only the I_n signal behaviour. Fig. 3 presents the I_n results for the first 7200 s of the immersion of the electrodes.

As indicated by the current-related data, the metastable pitting processes include pit initiation, rapid growth and slow repassivation [5]. As a consequence, these transients are characterised by a fast current rise followed by exponential decay which are often found in the pitting of carbon steel. It is important to stress out that the signal shape can vary for different metals [5]. Additionally, Lin et al. [29] have proposed that the number of transients is correlated

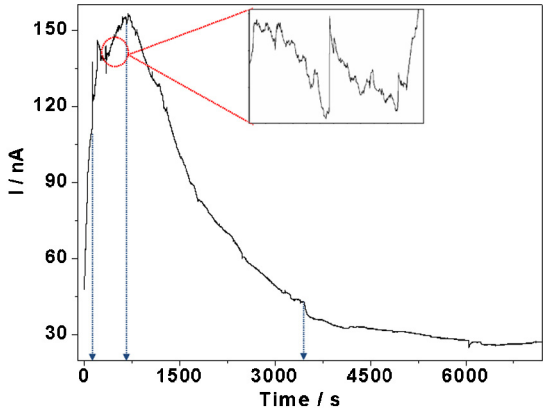

Fig. 3. Current electrochemical noise signals of the AISI 1020 steel in seawater, immediately after immersion.

to the number of inclusions and/or grain boundaries at the points where the pits start to grow once these defects become favoured sites for Cl^- adsorption. In Fig. 3, it is possible to observe intense current oscillations in the early stages, from 120 s up to approximately 665 s. This result can be explained by localized corrosion processes that occur on the different surface regions susceptible to this kind of attack, such as inclusions and grain boundaries. As well as the oscillatory characteristics of the current noise signal, the number of transients also indicates a large number of local attacks, as shown in the inset of Fig. 3.

Images captured at different times of the immersion are shown in Fig. 4. Initially, Fig. 4a shows the micrograph of a recent exposed steel in the seawater. In this case, there is no sign of corrosion, as expected. In Fig. 4b, after 1000 s of immersion, it is observed the formation of a brown film which partially covers the surface. Indeed, this Fig. 4b shows the moment where this film is continuously dissolved into the solution. After this process, film dissolution, in the central part of the micrograph, it is clear the initial corrosion of the surface at both grain boundaries and inclusions. Fig. 4c, after 2000 s of immersion, presents the final dissolution of the brown film which is still present at the borders of the electrode. Now it is also clear the present of a large number of inclusions which are corroded as well as the grain boundary corrosion. These data, are in agreement with ex situ micrograph presented in Fig. 1.

In Fig. 3, after the maximum current (at 665 s), it is observed a current decrease. Besides, current transients are still observed until 3470 s although their number continuously decreases. This point of the experiment is illustrated in Fig. 4d which brings the micrograph at 3470 s of immersion in the solution. It also observed final of the dissolution of the brown film. Considering the data obtained from the literature [3,30] and the results presented in Fig. 4b, c and d, there is the breakdown of a thin layer formed and the corrosion at inclusions and grain boundaries. Different mechanisms for the breakdown of oxide at the grain boundaries are proposed in the literature [30], depending on which interface governs the potential drop: (i) local thinning and dissolution of the oxide layer, (ii) metal voiding or (iii) particle growth at the metal/oxide interface followed by rupture of the barrier layer. Regardless of the mechanism that occurs during corrosion of the grain boundary, this process is also associated with current transients. Based on Figs. 3 and 4, it is then possible to propose that, in the region of the current decay observed in Fig. 3, two types of localized corrosion occur: pit formation and intergranular corrosion.

A micrograph of the surface after an immersion time in the solution of 2.2×10^4 s, Fig. 4e, shows an intensification of corrosion mainly at the grain boundary. There is also a darkening of the surface, which is possibly associated with the formation of a second oxide layer. These proposals are supported by the changes in the current noise profile, which is shown in Fig. 5a for an immersion time of between 1.8×10^4 and 2.5×10^4 s. During this period of time the characteristic noise signal could be associated both with localized, and also with the generalized corrosion processes. These results were in agreement with data in the literature where, in such cases, the noise frequency signal is high [16,31,32]. Noise frequency (f_n) appeared to be a promising parameter for monitoring changes in the corrosivity of the environment. In the high frequency region it reflects the activities of general corrosion at the surface. In contrast, it is proposed that low frequency events are related to localized corrosion. Thus f_n provides an indicator of the type of corrosion that is occurring, with a small f_n indicating localized corrosion and a large f_n indicating general corrosion.

The current noise signal profile shown in Fig. 5b, reached after an interval of 5.2×10^4 s, is characteristic of general corrosion, since it has a high f_n compared to the signal shown in Figs. 3 and 5a. The presence of this type of corrosion was confirmed by the

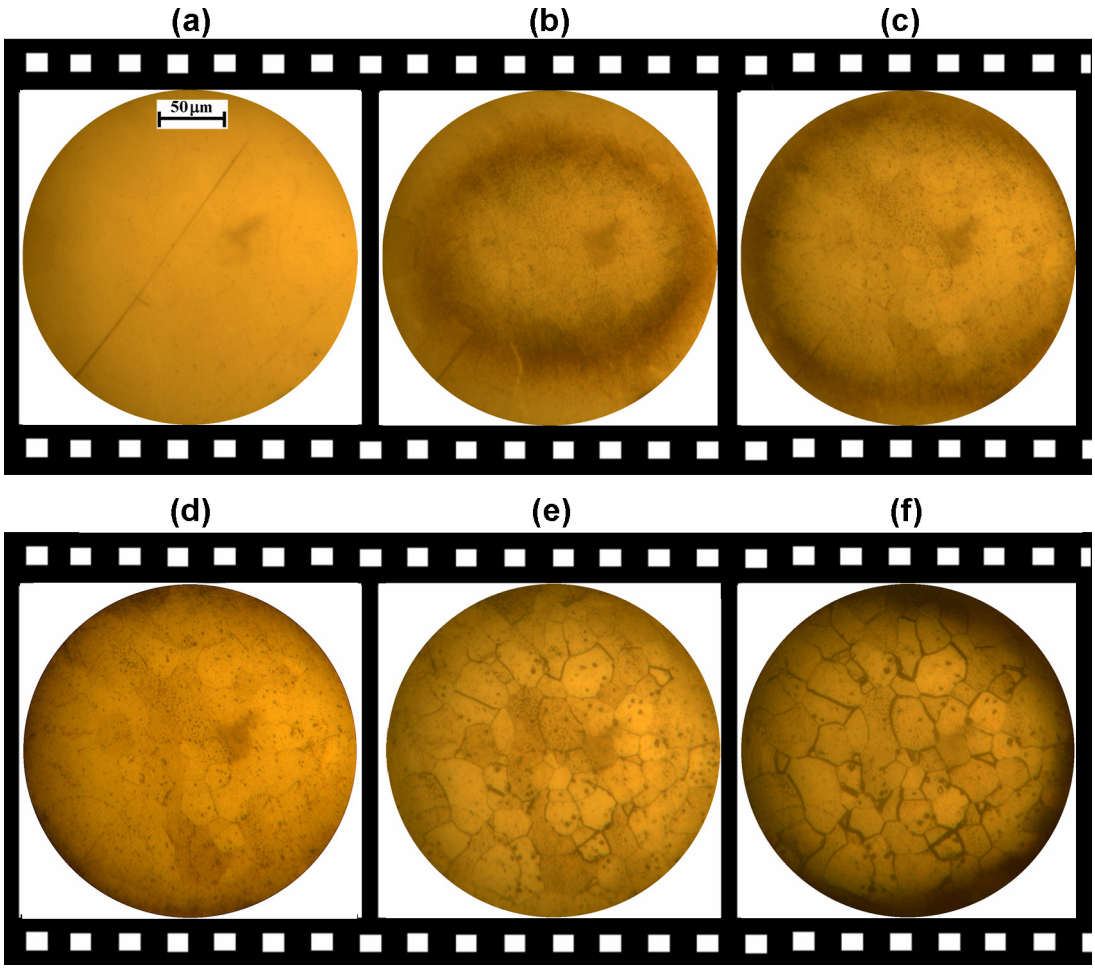

Fig. 4. Optical micrographs obtained of the WE_1 surface during acquisition of ECN data, at different times after immersion: (a) 1 s; (b) 1000 s; (c) 2000 s; (d) 3470 s; (e) 21,600 s; and (f) 50,400 s.

micrograph shown in Fig. 4f, in which it can be observed that grains of metal became darker because of the general corrosive attack. Once the carbon steel is in a corrosive environment, it is expected that corrosion occurs continuously. Initially, as demonstrated here, the regions most susceptible to corrosion are primordially attacked (impurities in the form of inclusions and grain boundaries). Since these regions are converted to stable corrosion products, it is expected that the intragrain regions themselves become the main active ones as the process continues.

It is not a simple assignment to describe subtle changes in the type of corrosion process investigated here using electrochemical noise current in the time domain plot. The transients can overlap with each other during simultaneous formation of two (or more) pits, leading to convoluted oscillations that can be incorrectly interpreted as multiple transients. There are several methods described in the literature for converting time domain data to make possible to obtain quantitative and qualitative information in a straightforward manner. Among these methods, as described in

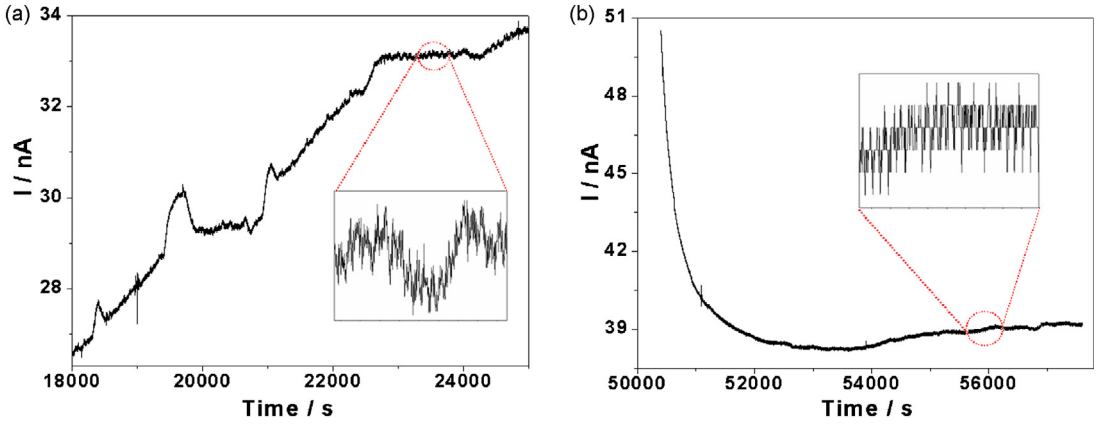

Fig. 5. Current electrochemical noise signals of the AISI 1020 steel in seawater: (a) after 18,000 s; and (b) after 51,000 s.

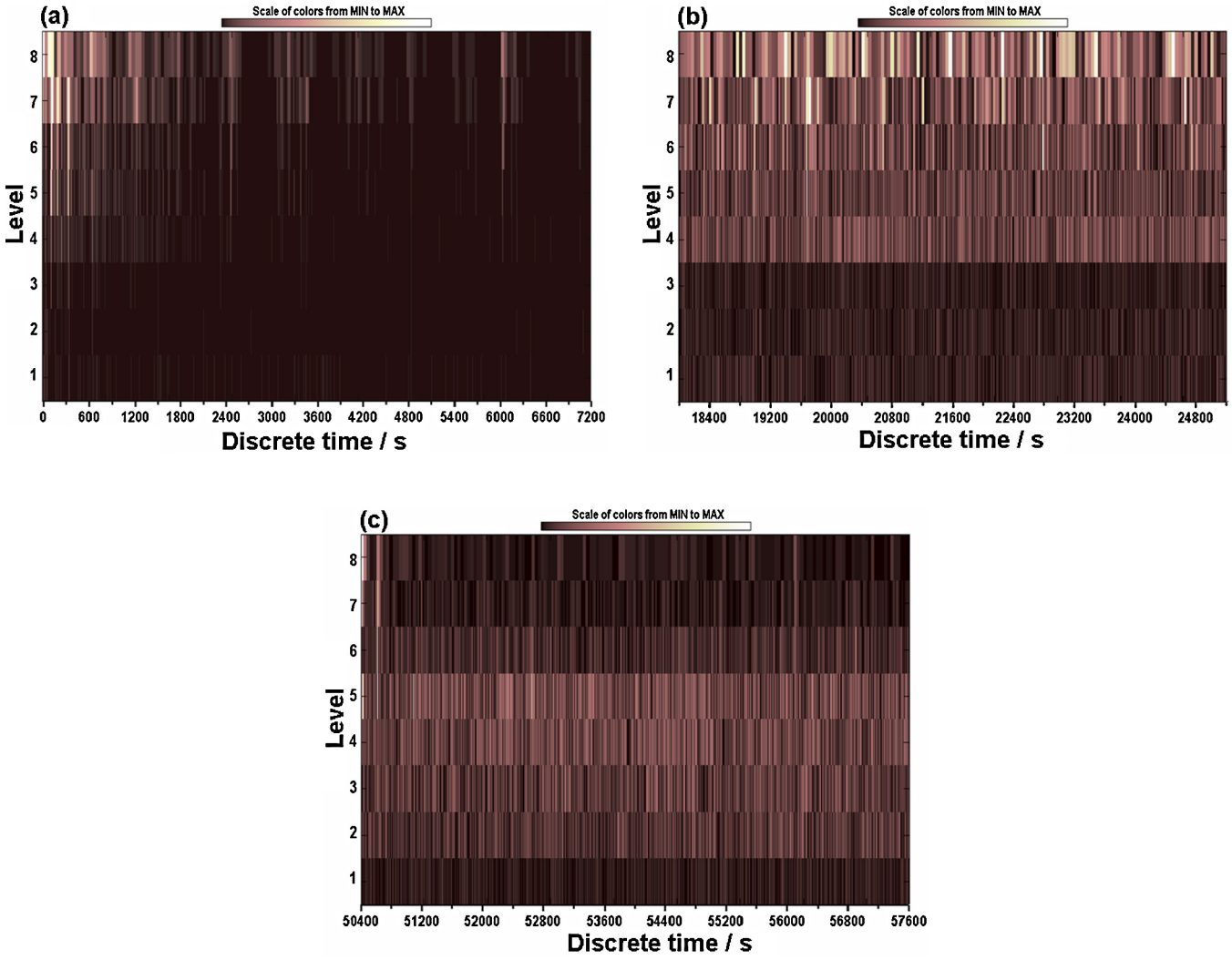

Fig. 6. Two-dimensional visual presentation of discrete time wavelet transforms of electrochemical noise current signals for AISI 1020 steel in seawater.

the Introduction to this paper, are Fourier transform and wavelets [5,16]. Using such transforms in the frequency domain clarifies these subtleties, making it possible to correlate the characteristic patterns of the signal with the chemical-physical phenomena [16,33–36]. Therefore, in order to separate the contributions of the different processes, wavelet transform was applied to the noise data in order to describe the corrosion processes studied in this work.

One form of presenting the results obtained by wavelet transform is to use two-dimensional diagrams, in which energy values are represented as a function of both discrete values of frequencies and of time. The two-dimensional time (serial number of the sampling point) and frequency (level, scale) representation are shown in Fig. 6. Each rectangle on the plane shows the corresponding wavelet coefficient, in greyscale code, with black representing the minimum and white representing the maximum value. In this type of representation, i.e., a discrete transform, sudden changes in the signal are evidenced as a clear region in the diagram, such as those which occur in the pitting formation or other localized processes.

The energy distribution, relative to the level coefficients, d_1–d_8, mainly reflects information concerning the processes of initiation (or development) of corrosion being investigated. In agreement with the literature [16], the levels from d_1–d_4 ($f > 3.8$ Hz) could be attributed to general corrosion, while the remaining levels, from d_5–d_8, could be associated with localized corrosion processes ($f < 3.8$ Hz), such as intergranular and pit formation. Fig. 6a particularly shows these processes at the beginning of the measurement, after 600 s, predominantly for levels d_7 and d_8. This means that a large number of current transients occur at the beginning of the measurements, as is also observed in Fig. 3.

In a different way, Fig. 6b shows that low frequencies, at levels d_4 to d_8, have an influence along the whole time interval. It is important to note that the greyscale in Fig. 6a, b and c is not comparable, because the principle of conservation of energy of the signal is applied to the analysed interval, and the energy contained is not necessarily equal for different intervals. Considering this point, the comparison of Fig. 6a and b makes possible to observe evidences of localized corrosion, which could be related to pitting and/or grain boundary processes. As discussed above, just from these data themselves, it is impossible to infer which one (pitting or grain boundary) is the main driver for the energy diagram data. However, using them combined together with in situ micrographs, it is possible to determine that pitting corrosion is the main process at the beginning of the experiment and that the contribution of grain boundary processes increases as the time of experiment increase. After 5.2×10^4 s, as illustrated in Fig. 6c, the profile is quite different. The light region, which contains the largest accumulation of energy, appears between levels d_2–d_5. Again, analysing these data together with those presented in Fig. 4 (especially Fig. 4f), one can

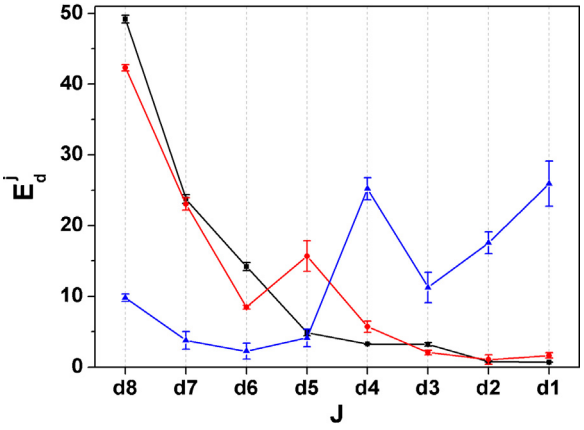

Fig. 7. Energy diagram plot corresponding to the electrochemical current noise signals for AISI 1020 steel in seawater, at different times after immersion: 0–2720 s (■); 4480–7200 s (●); and 52,000–54,720 s (▲). Error bars indicate the standard deviation from duplicate.

infer that general corrosion predominates in this last part of the experiment.

To summarise the wavelet transform results described in Fig. 6 in more detail, the energy (E_j), named here as the relative energy of a level, was calculated and plotted versus the relative level (J), and presented as an energy diagram plot (EDP; Fig. 7). The relative energy of a level, which is used to estimate the contribution to the overall energy made by the interval time of a signal in the analyses, can be calculated as shown in the literature [16].

From this representation, it is clear that, during the first hour (3600 s), there is a predominance of localized corrosion caused by the relative energy accumulated at d_6–d_8. At an interval time of 4480–7200 s, it can be observed that the energy contribution of localized processes begins to decline, indicating a change from one type of corrosion to another. This corroborates with the ending of punctual attack in the inclusions, as observed in the micrograph shown in Fig. 4. After 5.2×10^4 s, general corrosion can be observed to become predominant, as evidenced by the increase in cumulative energy in the d_1–d_4 levels.

In summary, comparing Figs. 3 and 7, it is possible to deduce that pitting corrosion was the main corrosion process initially developed, followed by grain boundary corrosion and then finally, general corrosion. Then, EDP can be used as a "fingerprint" of an ECN signal and to differentiate the type of corrosion. This result demonstrates the reliability of analysis when using complementary techniques.

4. Conclusions

The initial corrosion processes of AISI 1020 steel in seawater have been characterized by electrochemical noise coupled with in situ optical microscopy. A wavelet transform was employed to analyse the ECN data, and the energy distribution plot of the detailed wavelet coefficients was used to evaluate the activity of current transients at different time scales, enabling the identification of different types of corrosion. An important change in the type of corrosion was observed during the first hour of immersion. Initially, at approximately 3470 s, the corrosion was predominantly localised, due to pit formation. After this period, it could be observed from both the EDP and micrographs that intergranular corrosion had become dominant. After approximately 50,000 s (14 h) of immersion, general corrosion processes dominated.

The interpretation of signals by ECN and wavelets analysis was confirmed by optical micrographs, and this approach of coupled techniques can therefore be valuable to investigating corrosion, as some types of processes are often not identified when these techniques are employed separately. Finally, it was possible to make qualitative and quantitative analyses of the changes occurring to the type of corrosion during the onset of corrosion on steel.

Acknowledgements

The authors would like to thank FAPESP (Proc.: 98/14324-0, 11/19430-0), CNPq and CAPES for financial support.

References

[1] N. Perez, Electrochemistry and Corrosion Science, Kluwer Academic Publishers, Boston, 2004.
[2] J.L. Dawson, Electrochemical Noise Measurement for Corrosion Applications, ASTM STP 1277, 1999.
[3] M. Hashimoto, S. Miyajima, T. Murata, A stochastic analysis of potential fluctuation during passive film breakdown and repair on iron, Corrosion Science 33 (1992) 885–904.
[4] Z. Shi, G. Song, C. Cao, H. Lin, M. Lu, Electrochemical potential noise of 321 stainless steel stressed under constant strain rate testing conditions, Electrochimica Acta 52 (2007) 2123–2133.
[5] Y.F. Cheng, J.L. Luo, M. Wilmott, Spectral analysis of electrochemical noise with different transient shapes, Electrochimica Acta 45 (2000) 1763–1771.
[6] G. Qiao, J. Ou, Corrosion monitoring of reinforcing steel in cement mortar by EIS and ENA, Electrochimica Acta 52 (2007) 8008–8019.
[7] Z.H. Dong, W. Shi, X.P. Guo, Initiation and repassivation of pitting corrosion of carbon steel in carbonated concrete pore solution, Corrosion Science 53 (2011) 1322–1330.
[8] N. Acuña-González, E. García-Ochoa, J. González-Sánchez, Assessment of the dynamics of corrosion fatigue crack initiation applying recurrence plots to the analysis of electrochemical noise data, International Journal of Fatigue 30 (2008) 1211–1219.
[9] M. Gomez-Duran, D.D. Macdonald, Stress corrosion cracking of sensitized Type 304 stainless steel in thiosulphate solution. II. Dynamics of fracture, Corrosion Science 48 (2006) 1608–1622.
[10] G.L. Edgemon, M.J. Danielson, G.E.C. Bell, Detection of stress corrosion cracking and general corrosion of mild steel in simulated defense nuclear waste solutions using electrochemical noise analysis, Journal of Nuclear Materials 245 (1997) 201–209.
[11] M. Kiwilszo, J. Smulko, Pitting corrosion characterization by electrochemical noise measurements on asymmetric electrodes, Journal of Solid State Electrochemistry 13 (2009) 1681–1686.
[12] F.H. Cao, Z. Zhang, J.X. Su, Y.Y.J. Shi, Q. Zhang, Electrochemical noise analysis of LY12-T3 in EXCO solution by discrete wavelet transform technique, Electrochimica Acta 51 (2006) 1359–1364.
[13] J. Smulko, K. Darowicki, A. Zielinski, Detection of random transients caused by pitting corrosion, Electrochimica Acta 47 (2002) 1297–1303.
[14] M.G. Pujar, N. Parvathavarthini, R.K. Dayal, S. Thirunavukkarasu, Assessment of intergranular corrosion (IGC) in 316(N) stainless steel using electrochemical noise (EN) technique, Corrosion Science 51 (2009) 1707–1713.
[15] S. Girija, U.K. Mudali, V.R. Raju, R.K. Dayal, H.S. Khatak, B. Raj, Determination of corrosion types for AISI type 304L stainless steel using electrochemical noise method, Materials Science and Engineering A 407 (2005) 188–195.
[16] A. Aballe, M. Bethencourt, F. Botana, M. Marcos, Using wavelets transform in the analysis of electrochemical noise data, Electrochimica Acta 44 (1999) 4805–4816.
[17] B. Zhao, J.H. Li, R.G. Hu, R.G. Du, C.J. Lin, Study on the corrosion behavior of reinforcing steel in cement mortar by electrochemical noise measurements, Electrochimica Acta 52 (2007) 3976–3984.
[18] L. Liu, Y. Li, F. Wang, Pitting mechanism on an austenite stainless steel nanocrystalline coating investigated by electrochemical noise and in-situ AFM analysis, Electrochimica Acta 54 (2008) 768–780.
[19] G.S. Frankel, Pitting corrosion of metals: A review of the critical factors, Journal of the Electrochemical Society 145 (1998) 2186–2198.
[20] N.D. Budiansky, L. Organ, J.L. Hudson, J.R. Scully, Detection of interactions among localized pitting sites on stainless steel using spatial statistics, Journal of the Electrochemical Society 152 (2005) B152–B160.
[21] Y. Li, R. Hu, J. Wang, Y. Huang, C. Lin, Corrosion initiation of stainless steel in HCl solution studied using electrochemical noise and in-situ atomic force microscope, Electrochimica Acta 54 (2009) 7134–7140.
[22] Y. Yin, L. Niu, M. Lu, W. Guo, S. Chen, In situ characterization of localized corrosion of stainless steel by scanning electrochemical microscope, Applied Surface Science 255 (2009) 9193–9199.
[23] M.M. Amin, S.S. Abdelrehim, A.E. Elsherbini, AC and DC studies of the pitting corrosion of Al in perchlorate solutions, Electrochimica Acta 51 (2006) 4754–4764.
[24] C. Punckt, M. Bölscher, H.H. Rotermund, A.S. Mikhailov, L. Organ, N. Budiansky, J.R. Scully, J.L. Hudson, Sudden onset of pitting corrosion on stainless steel as a critical phenomenon, Science 305 (2004) 1133–1136.
[25] A.M. Zimer, E.C. Rios, P.C. Mendes, W.N. Gonçalves, O.M. Bruno, E.C. Pereira, L.H. Mascaro, Investigation of AISI 1040 steel corrosion in H2S solution containing

chloride ions by digital image processing coupled with electrochemical techniques, Corrosion Science 53 (2011) 3193–3201.
[26] J. Lyman, R.H. Fleming, Composition of sea water, Journal of Marine Research 3 (1940) 134–146.
[27] L. Organ, J.R. Scully, A.S. Mikhailov, J.L. Hudson, A spatiotemporal model of interactions among metastable pits and the transition to pitting corrosion, Electrochimica Acta 51 (2005) 225–241.
[28] Y. Cheng, M. Wilmott, J. Luo, The role of chloride ions in pitting of carbon steel studied by the statistical analysis of electrochemical noise, Applied Surface Science 152 (1999) 161–168.
[29] B. Lin, R. Hu, C. Ye, Y. Li, C. Lin, A study on the initiation of pitting corrosion in carbon steel in chloride-containing media using scanning electrochemical probes, Electrochimica Acta 55 (2010) 6542–6545.
[30] P. Marcus, V. Maurice, H.-H. Strehblow, Localized corrosion (pitting): A model of passivity breakdown including the role of the oxide layer nanostructure, Corrosion Science 20 (2008) 2698–2704.
[31] H.A.A. Al-Mazeedi, R.A. Cottis, A practical evaluation of electrochemical noise parameters as indicators of corrosion type, Electrochimica Acta 49 (2004) 2787–2793.
[32] A. Legat, V. Dolecek, Chaotic analysis of electrochemical noise measured on stainless steel, Journal of the Electrochemical Society 142 (1995) 1851–1858.
[33] J.J. Kim, Wavelet analysis of potentiostatic electrochemical noise, Materials Letters 61 (2007) 4000–4002.
[34] M. Attarchi, M.S. Roshan, S. Norouzi, S. Sadrnezhaad, A. Jafari, Electrochemical potential noise analysis of Cu–BTA system using wavelet transformation, Journal of Electroanalytical Chemistry 633 (2009) 240–245.
[35] A.M. Homborg, T. Tinga, X. Zhang, E.P.M.V. Westing, P.J. Oonincx, J.H.W.D. Wit, J.M.C. Mol, Time–frequency methods for trend removal in electrochemical noise data, Electrochimica Acta 70 (2012) 199–209.
[36] P. Planinsic, Petek, Characterization of corrosion processes by current noise wavelet-based fractal and correlation analysis, Electrochimica Acta 53 (2008) 5206–5214.